

# Probing the onset of hydrodynamization in peripheral p-Pb collisions at $\sqrt{s_{NN}} = 5.02$ TeV

Nikhil Hatwar,\* Sadhana Dash, and Basanta Kumar Nandi  
*Indian Institute of Technology, Bombay, Powai, Mumbai, India*  
(Dated: October 29, 2024)

An attempt has been made to estimate the minimum size of the de-confined matter of Quark-Gluon Plasma (QGP) in small system that could be satisfactorily modeled with low-order hydrodynamics. The elliptic flow coefficient has been studied for the variation of second order transport coefficient called the shear relaxation time, which acts as a regulator of the non-hydrodynamic mode of theory. The small system of p-Pb collision at  $\sqrt{s_{NN}} = 5.02$  TeV is simulated on the state-of-art framework of JETSCAPE. We modeled the soft sector dynamics using an initial condition, a pre-equilibrium stage, hydrodynamics and a hadron afterburner. We generated results of transverse momentum spectra and rapidity spectra of light particles to match the simulated system with the experimental data. We looked at elliptic flow variation for extreme values of shear relaxation time for peripheral collision centralities. The increase in elliptic flow fluctuations indicate breakdown of fluid behavior at around  $dN/dy \approx 8$  for p-Pb collision at  $\sqrt{s_{NN}} = 5.02$  TeV.

## I. INTRODUCTION

Over the last few decades, we have slowly gathered mounting indirect evidence of the production of a de-confined quark matter in relativistic heavy-ion collisions carried out at BNL's Relativistic Heavy Ion Collider and CERN's Large Hadron Collider [1, 2]. The focus is now shifting towards finding the properties of this phase of strongly interacting matter. But simultaneously, the discovery of most of these Quark-Gluon Plasma (QGP) signatures in small systems like proton-nucleus and high multiplicity proton-proton collisions has been puzzling [3–6].

Currently are confronted with the question of whether these signatures are a result of cold nuclear matter effects [7], genuine QGP-like hot nuclear matter effects [8], or is it something in-between [9]. Fig. 1 shows a cartoon of collision domains for varying atomic mass (which represents the system size of collision) and collisional energy. In the domain of large collisional energy and large system size, we have convincing evidence of QGP formation, shown as a large red blob. At low collisional energy, we have nucleon and/or parton scattering off each other, represented by blue color. There is no consensus about the nature of medium produced for smaller system size and large collisional energy, represented by three red circles in Fig. 1. There should lie a threshold value of collisional energy for a suitably large collision system beyond which hot QCD matter could form [10, 11]. If we do not have deconfined medium in small systems like proton-proton at large energies, there should lie another threshold of system size for which hot QCD matter could form. In the present study, we are trying to estimate this system size threshold marked as *system size deconfinement onset* in Fig. 1 for peripheral p-Pb collisions at  $\sqrt{s_{NN}} = 5.02$  TeV.

Relativistic hydrodynamics has emerged as a key effective dynamics in modeling the QGP phase of high energy collisions [12]. The early phenomenological success of hydrodynamic description for collective expansions in the heavy-ion collisions indicated the formation of locally equilibrated isotropic matter as early as  $1 \text{ fm}/c$  [13]. But no theoretical approach came even close to explaining such a rapid transition from strong color field configuration to a locally thermalized system of quarks and gluons [14]. It is also found that starting from various initial conditions, evolution of pressure anisotropy is accurately described by hydrodynamic gradient expansion. This surprising result indicates that the phenomenological success of hydrodynamics does not necessarily require early thermalization or even isotropization in the heavy-ion collisions [15]. Hence, a more appropriate question to ask would be: how far away from equilibrium, would hydrodynamics still be applicable [16, 17]? Previous studies have explored different ways to address this question using entropy density [18] and collective flow related observables [19].

For a long time, hydrodynamics has been associated with an equilibrium state. But now, since the system under consideration is strictly not in local thermal equilibrium, the word "hydrodynamization" was coined by Casalderrey-Solana, Liu et al. [20] to distinguish the low-order viscous hydrodynamic constitutive relations from local thermalization. The usual approach to hydrodynamics involves expansion of the energy-momentum tensor in terms of gradients of fields. Here, the fundamental hydrodynamic fields are considered in the local rest frame to build the energy-momentum tensor ( $T^{\mu\nu}$ ) of the system, which is then put into the conservation equation ( $\partial_\mu T^{\mu\nu} = 0$ ). With just the fields in energy-momentum tensor expression, we have the zeroth order of ideal hydrodynamics. If we also include the first-order gradient which represents the dissipative effects, we run into the causality violation problem of Navier Stokes equation[21]. Few studies have made progress in restoring causality at first order [22, 23]. At second-order gradient, different

\* nikhil.hatwar@gmail.com

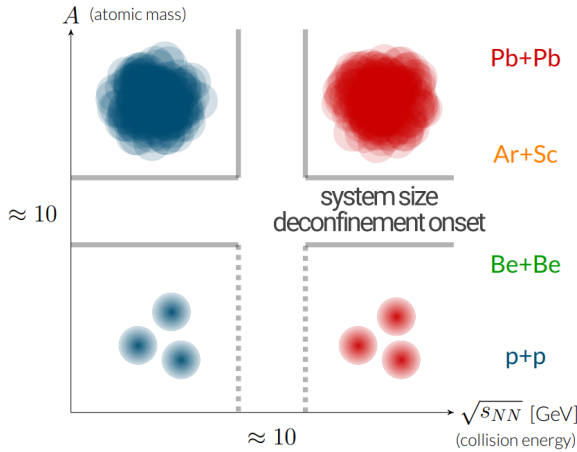


FIG. 1. Cartoon of collision domains for varying atomic mass and collisional energy. The three blue circles and the large blue blob at low collisional energy represent cold nuclear matter. The large red blob represents the QGP formation regime. The three small red circles represent a region where the nature of QCD matter produced is debatable. Figure adapted from Ref. [30].

formalisms keep different number/kind of term, resulting in variations, e.g., MIS [24–26], DNMR [27], aHydro [28], BRSSS [29].

There are signs that this familiar hydrodynamic gradient expansion is generally not a convergent series [16]. To examine the collective modes of diverging gradient expansion, we usually consider the linear response of the energy-momentum tensor ( $T^{\mu\nu}$ ) due to an arbitrary perturbing source,  $S_{\gamma\delta}$  as [31],

$$\delta\langle T^{\mu\nu} \rangle(t, \mathbf{x}) = \int dt d^3x G^{\mu\nu, \gamma\delta}(t, \mathbf{x}) S_{\gamma\delta}, \quad (1)$$

where  $G^{\mu\nu, \gamma\delta}(t, \mathbf{x})$  is the two-point retarded correlator, referred to as Green's function. The solution of this equation at late times is expressed in the form,

$$\delta\langle T^{\mu\nu} \rangle(t, \mathbf{x}) \sim e^{-i\omega_{\text{sing}}(k)t + i\mathbf{k}\cdot\mathbf{x}}, \quad (2)$$

where  $\omega_{\text{sing}}(k)$  is the complex singularity of Fourier transformed two-point retarded correlator. The real part of this complex frequency is termed “hydrodynamic mode frequency” which is responsible for the excitation of equilibrium plasma. And the imaginary part is referred to as “non-hydrodynamic mode frequency”, which causes dissipative effects. For BRSSS theory, these singularities have been worked out for sound channel [32] with the hydrodynamic mode frequency given as,

$$\omega_h^\pm = \pm \frac{k}{\sqrt{3}} - \frac{2i\eta k^2}{3Ts} + \dots \quad (3)$$

and the corresponding non-hydrodynamic mode frequency is given by,

$$\omega_{\text{nh}} = -i \left( \frac{1}{\tau_\pi} - \frac{4\eta k^2}{3sT} \right) + \dots \quad (4)$$

In the above equations 3 and 4,  $\eta$  is shear viscosity,  $T$  is temperature,  $s$  is entropy density,  $k$  is the wave vector and  $\tau_\pi$  is the second order transport coefficient called shear relaxation time. For vanishing wave vector these frequencies reduce to,

$$\lim_{k \rightarrow 0} \omega_h^\pm = 0 \quad ; \quad \lim_{k \rightarrow 0} \omega_{\text{nh}} = -\frac{i}{\tau_\pi} \quad (5)$$

The fact that  $\omega_{\text{nh}}$  cannot be eliminated in the limit of  $k \rightarrow 0$  is the defining feature of non-hydrodynamic mode.

The contemporary understanding of hydrodynamics indicates that the applicability of hydrodynamics is exclusively determined by the contribution of non-hydrodynamic mode relative to hydrodynamic mode. The fluid behavior will break down if the contribution of non-hydrodynamic mode exceeds that of hydrodynamic mode. The non-hydrodynamic mode is regulated by the second-order transport coefficient called shear relaxation time, as seen in Eq. 4.

The idea is to study the behavior of elliptic flow for the extreme values of shear relaxation time for peripheral collisions in p-Pb collisions at  $\sqrt{s_{\text{NN}}} = 5.02 \text{ TeV}$ . An abrupt deviation in elliptic flow would signify a breakdown of hydrodynamic behavior as suggested by Paul Romatschke [16]. In the previous study [33], we looked at the onset of hydrodynamization for peripheral Pb-Pb collisions at  $\sqrt{s_{\text{NN}}} = 2.76 \text{ TeV}$  and Au-Au collisions at  $\sqrt{s_{\text{NN}}} = 200 \text{ GeV}$  and the onset was found roughly at  $dN/dy \approx 10$ .

The structure of this paper is as follows. In Sec. II we explain the motivation of using the new framework and a brief description of models utilized for different collision stages. The choice of parameter and the benchmarking of model for available experimental data is explained in Sec. III. In Sec. IV we provide results for elliptic flow as a function of  $p_T$  and  $dN/dy$  using two methods of varying the shear relaxation time, followed by summary in Sec. V.

## II. MODEL FRAMEWORK

To simulate the soft sector of p-Pb collisions at  $\sqrt{s_{\text{NN}}} = 5.02 \text{ TeV}$ , one could select separate models designed for pre-equilibrium, fluid, and hadron afterburner stages individually and use them in tandem. To ensure that these models are used in a compatible way, a comprehensive framework has recently been developed called JETSCAPE [34]. This modular framework has shown promising results with the possibility of simulating both the regimes of dynamics viz. soft and hard sector as well as their interaction in recent studies [35–39]. With all models put under one framework, the possibility of seamlessly reproducing and comparing studies investigating widely different aspects has opened up. In addition to the above, multi-signature studies could be performed in the future providing a holistic picture of quark matter in high energy collisions. For the study presented in this paper, we have employed JETSCAPE 3.6.4 [40]. The

dynamics used is 2+1 dimensional as it has shown satisfactory agreement with its 3+1 dimensional counterpart at midrapidity [41]. The individual stage modules selected are [ T<sub>RENT</sub>O + Freestreaming + MUSIC + iSS + SMASH ]. A very brief description of each of these modules is given below:

### A. Initial condition: T<sub>RENT</sub>O

The T<sub>RENT</sub>O model [42] generates initial energy density deposited in the plane transverse to the motion of approaching nuclei right after they have crossed each other without assuming any underlying physical dynamics. To begin with, nucleon positions in the approaching nuclei A and B are randomly sampled from Woods-Saxon distribution while ensuring a minimum distance ( $d_{min}$ ) between nucleons, to account for repulsive forces between them. Individual nucleon density is assumed to be of Gaussian form,

$$\rho_n(\mathbf{x}) = \frac{1}{(2\pi w^2)^{3/2}} \exp\left(-\frac{|\mathbf{x}|^2}{2w^2}\right), \quad (6)$$

where the standard deviation,  $w$  is a T<sub>RENT</sub>O parameter which signifies the effective nucleon width. The T<sub>RENT</sub>O model considers constituents in nucleons in a similar way as the nucleons in a nucleus [43]. Consider a nucleon-nucleon collision at a given impact parameter,  $\mathbf{b}_n$ . The density in Eq. 6 of a single nucleon is used to find nucleon thickness function,  $T_n(\mathbf{x}_\perp) = \int dz \rho_n(\mathbf{x}_\perp, z)$ , which is then used to calculate the nucleon-nucleon overlap function,

$$T_{nn}(\mathbf{b}_n) = \int d^2x T_n(\mathbf{x}_\perp) T_n(\mathbf{x}_\perp - \mathbf{b}_n). \quad (7)$$

The collision probability of at least one nucleon-nucleon pairwise interaction is given as [44],

$$P_{nn}^{coll}(\mathbf{b}_n) = 1 - \exp[-\sigma_{\text{eff}}^{\text{inel}} T_{nn}(\mathbf{b}_n)], \quad (8)$$

where  $\sigma_{\text{eff}}^{\text{inel}}$  is the effective cross section of interaction between nucleon constituents. Starting with this, we find the *number of participating nucleons* ( $N_{\text{part}}$ ) from both nuclei<sup>1</sup>. The nucleon density given by Eq.(6) is summed over the number of participating nucleons to calculate nuclear density as,

$$\tilde{\rho}_A^{\text{part}}(\mathbf{x}) = \sum_{i=1}^{N_{\text{part}}^A} \gamma_i \rho_n(\mathbf{x} - \mathbf{x}_i + \mathbf{b}/2) \quad (9)$$

<sup>1</sup> From analytical Glauber model, the probability of *n nucleon-nucleon collision* is calculated using the single nucleon-nucleon collision probability,  $P_{nn}^{coll}(\mathbf{b}_n)$  of Eq.(8). And using that, one can find the average number of nucleons that participate in more than one pairwise collisions ( $N_{\text{part}}^A$  and  $N_{\text{part}}^B$ ) from each nucleus A and B [45]

Here,  $N_{\text{part}}^A$  is the number of participating nucleons from nucleus A,  $\mathbf{b}$  is the nucleus-nucleus collision impact parameter and  $\gamma_i$  is a weight factor sampled from a gamma distribution to introduce fluctuations like that in between events in the experimental setup [46]. An analogous equation is used for nucleus B with a negative sign for  $\mathbf{b}/2$  term. This fluctuating nuclear density then goes into calculating the nuclear thickness function,  $\tilde{T}_A(\tilde{x}_\perp) = \int dz \tilde{\rho}_A(\mathbf{x}_\perp, z)$ . The nuclear overlap function is calculated using a generalized mean called as *reduced thickness*,

$$T_R = \left( \frac{\tilde{T}_A^p + \tilde{T}_B^p}{2} \right)^{1/p}, \quad (10)$$

where  $p$  is a dimensionless real-valued parameter. The specific values of  $p = -1, 0, +1$  correspond to arithmetic, geometric and harmonic mean respectively as stated in Ref. [42]. This *reduced thickness* is then scaled with a normalization factor to obtain the initial energy deposited after the nucleus-nucleus collision.

### B. Pre-equilibrium: Freestreaming

The pre-equilibrium stage is intended to fill the gap between the initial stage of collision and the beginning of the near-equilibrium hydrodynamic stage with out-of-equilibrium dynamics. The approaching nuclei cross each other in time,  $\tau \approx 2R/\gamma\beta$ , where  $R$  is the rest frame radius of the nucleus,  $(2R/\gamma)$  is the Lorentz contracted length and  $\beta = v/c$ . For LHC and RHIC, this crossing time is of the order of  $10^{-3}$  fm/c and  $10^{-1}$  fm/c respectively. Crossing time is an appropriate moment to initiate the pre-equilibrium dynamics. But there is no such rationale for deciding the end time of pre-equilibrium dynamics or hydrodynamics starting time<sup>2</sup>. The role and effect of the pre-equilibrium stage on the final stage observables need to be looked at in more detail. The Freestreaming module used as a pre-equilibrium stage for this study is based on the collisionless Boltzmann equation of massless particles [36],

$$p^\mu \partial_\mu f(X; P) = 0, \quad (11)$$

where  $f(X; P)$  is the phase space momentum distribution of particles in the plane transverse to beam direction at the time of collision. This distribution is assumed to be locally isotropic. The solution of the above Boltzmann equation for a boost invariant system is calculated in terms of the moment of the distribution  $f(X; P)$  which is given as,

$$F[X; \Omega_p] \equiv \frac{g}{(2\pi)^3} \int P_0^3 f(X; P) dP_0, \quad (12)$$

<sup>2</sup> Other than finding the value of this time parameter which leads to satisfactory agreement between produced observables with experimental data.

where  $\Omega_p$  is the solid angle in momentum space,  $g$  is a degeneracy factor and  $P^0 = |\mathbf{P}|$ . We are interested in calculating energy-momentum tensor for this kinetic theory which will be evolved for the Freestreaming duration and then subsequently matched with the fluid energy-momentum tensor at the start of hydrodynamics. The Freestreaming energy-momentum tensor is expressed using the above moment as,

$$T^{\mu\nu}(t, \mathbf{x}) = \int \hat{p}^\mu \hat{p}^\nu F[t_0, \mathbf{x} - \mathbf{v}(t-t_0); \Omega_p] d\Omega_p, \quad (13)$$

where,  $t_0$  is the time at which we start the Freestreaming module.

The initial condition for  $T^{\mu\nu}$  is set through the initial energy density obtained from the TRENTo module as,

$$T^{00}(t_0, \mathbf{x}) = \epsilon = \mathcal{N}F(t_0, \mathbf{x}), \quad (14)$$

where  $\mathcal{N}$  is  $2\pi$  for the 2-dimensional momentum distribution. The evolution is stopped at freestreaming time,  $\tau_{fs}$ , which is also the time when the hydrodynamic module is initiated. The complete  $T^{\mu\nu}$  of pre-equilibrium stage is smoothly and consistently matched to the fluid stage in local rest frame using the Landau matching condition,

$$u_\mu T_\nu^\mu = \epsilon u_\nu. \quad (15)$$

This includes matching the viscous dissipative part of the tensor as well. The Freestreaming module is equipped with a feature to use centrality-dependent Freestreaming time,  $\tau_{fs}$ , given as,

$$\tau_{fs} = \tau_R \left( \frac{\langle \bar{\epsilon}_{\text{cent}} \rangle}{\bar{\epsilon}_R} \right)^\alpha. \quad (16)$$

Here,  $\langle \bar{\epsilon}_{\text{cent}} \rangle$  is the average transverse energy density of a given centrality,  $\epsilon_R$  is the normalization used for the duration for which Freestreaming operates,  $\alpha$  controls the contribution of initial energy density and  $\bar{\epsilon}_R$  is an arbitrary energy density reference.

### C. Viscous Hydrodynamics: MUSIC

MUSIC [47] is a second-order dissipative fluid dynamics based in BRSSS formalism [48] and uses the Landau choice of velocity rest frame, same as in Eq.(15). It has been widely used in phenomenological studies for various collision systems and energies [49]. The equation of state employed for this study matches with lattice QCD prediction [50]. The energy-momentum tensor conservation equations,  $\partial_\mu T^{\mu\nu} = 0$ , in MUSIC are solved using Kurganov-Tadmor algorithm [47]. The fluid energy-momentum tensor is constructed using the ideal fluid part,  $T^{\mu\nu} = \epsilon u^\mu u^\nu + \Delta^{\mu\nu} P$  and a dissipative part,  $\Pi^{\mu\nu}$ . It is customary to split this dissipative tensor further into traceless and trace parts,  $\Pi^{\mu\nu} = \pi^{\mu\nu} + \Pi\Delta^{\mu\nu}$  which are referred to as shear and bulk part of dissipative tensor, respectively. The term,  $\Delta^{\mu\nu} \equiv g^{\mu\nu} - u^\mu u^\nu$ ,

projects onto the spatial part in the local rest frame. For MUSIC, the evolution equation for shear tensor is given as:

$$\begin{aligned} \tau_\pi \dot{\pi}^{\langle\mu\nu\rangle} + \pi^{\mu\nu} &= 2\eta\sigma^{\mu\nu} - \delta_{\pi\pi}\pi^{\mu\nu}\partial_\lambda u^\lambda + \varphi_7\pi_\alpha^{\langle\mu}\pi^{\nu\rangle\alpha} \\ &\quad - \tau_{\pi\pi}\pi_\alpha^{\langle\mu}\sigma^{\nu\rangle\alpha} + \lambda_{\pi\Pi}\Pi\sigma^{\mu\nu}. \end{aligned} \quad (17)$$

The evolution for the bulk term is given as,

$$\tau_\Pi \dot{\Pi} + \Pi = -\zeta\partial_\lambda u^\lambda - \delta_{\Pi\Pi}\Pi\partial_\lambda u^\lambda + \lambda_{\Pi\pi}\pi^{\mu\nu}\sigma_{\mu\nu}, \quad (18)$$

where  $\dot{\Pi} = u^\lambda\partial_\lambda\Pi$ ,  $\dot{\pi}^{\langle\mu\nu\rangle} = \Delta_{\alpha\beta}^{\mu\nu}u^\lambda\partial_\lambda\pi^{\alpha\beta}$ , and  $\sigma^{\mu\nu} = \Delta_{\alpha\beta}^{\mu\nu}\partial^\alpha u^\beta$ , with  $\Delta_{\alpha\beta}^{\mu\nu}$  is a projector that takes out part of a rank-2 tensor, that is traceless, symmetric, orthogonal to velocity  $u^\mu$  and is given as:

$$\Delta_{\alpha\beta}^{\mu\nu} \equiv \frac{1}{2}(\Delta_\alpha^\mu\Delta_\beta^\nu + \Delta_\alpha^\nu\Delta_\beta^\mu) - \frac{1}{3}\Delta^{\mu\nu}\Delta_{\alpha\beta}. \quad (19)$$

Where  $\delta_{\Pi\Pi}$ ,  $\lambda_{\Pi\pi}$ ,  $\delta_{\pi\pi}$ ,  $\varphi_7$ ,  $\tau_{\pi\pi}$ , and  $\lambda_{\pi\Pi}$ ,  $\tau_\pi$  and  $\tau_\Pi$  are the second order transport coefficients, which depends upon the details of underlying microscopic theory under consideration [51].

The first-order transport coefficients, shear, and bulk viscosities are conventionally introduced by taking the ratio with the entropy density. In a realistic scenario, the shear viscosity to entropy density ratio ( $\eta/s$ ) would be a function of temperature. Constraints on this temperature-dependent  $\eta/s$  have been explored in a Bayesian study [52]. The temperature dependent  $\eta/s$  in this work has been parameterized as [36],

$$\begin{aligned} \frac{\eta}{s}(T) &= a_{\text{low}}(T - T_\eta)\Theta(T_\eta - T) + (\eta/s)_{\text{kink}} \\ &\quad + a_{\text{high}}(T - T_\eta)\Theta(T - T_\eta). \end{aligned} \quad (20)$$

Here,  $\Theta$  is the Heaviside step function,  $a_{\text{high}}$ ,  $a_{\text{low}}$ ,  $(\eta/s)_{\text{kink}}$  and  $T_\eta$  are the parameters chosen such that  $\eta/s$  stays with the bounds allowed by Bayesian analysis. The second order transport coefficient called *shear relaxation time*,  $\tau_\pi$ , is related to  $\eta/s$  as,

$$\tau_\pi(T) = \frac{b_\pi}{T} \frac{\eta}{s}(T) \quad (21)$$

where  $b_\pi$  is a constant whose values have been estimated from microscopic theories. The fluid dynamics stops when the system has cooled enough for hadronization to take place. During the hadronization process, the free quarks and gluons recombine into hadrons below the pseudocritical temperature of roughly 156 MeV [53].

### D. Hadron afterburner: (iSS + SMASH)

When the fluid cell temperature drops below the particlization temperature<sup>3</sup>, a hypersurface of fluid cells is

<sup>3</sup> particlization is the point at which the fluid description is stopped and particles are introduced at freezeout.

created. A hypersurface is a spacetime volume of fluid that has attended the particlization temperature. The hydrodynamic fields at this hypersurface are converted into particles using the Cooper-Frye prescription [54],

$$E \frac{d^3 N_i}{dp^3} = \frac{dN_i}{p_T dp_T dy d\phi_p} = g_i \int_{\Sigma} f_i(u^\mu p_\mu) p_\mu d\Sigma_\mu \quad (22)$$

This prescription has been used as an effective description for the least understood hadronization process which should happen over some duration during a mixed phase of hadrons and yet-to-be-hadronized partons. Eq.(22) gives the spectra of particles (in a near-equilibrium state) of species  $i$  at the hypersurface denoted by  $\Sigma$  in the direction normal to hypersurface. The coefficient  $g_i$  is the degeneracy factor of species  $i$ .

The quantity,  $f_i(u^\mu p_\mu)$  is the phase space distribution of particles generated. The information about hydrodynamic fields goes into this distribution through the Lorentz invariant energy expression  $E = u^\mu p_\mu$ . The form of this distribution has to be guessed such that the energy-momentum tensor from the fluid description at the point of particlization would match that of the subsequent kinetic transport. The usual choice of the local equilibrium part of this distribution is,

$$f(u^\mu p_\mu) = \frac{1}{(2\pi)^3} \frac{1}{\exp[(u^\mu p_\mu - \mu_i)/T_{sw}] \pm 1}, \quad (23)$$

where  $\mu_i$  is the equilibrium chemical potential of species  $i$ . If there are other charges considered, their chemical potential can be obtained by summing over the product of their corresponding charge and chemical potentials. To capture the out-of-equilibrium dissipative nature of fluid translated into particle description, a correction to this phase space distribution should be added.

In the framework of this study, particles are sampled from random positions on the hypersurface. This is handled by the iSS package [55]. For peripheral collisions, where multiplicity is small, there is a feature to sample particles more than once. This helps in increasing the particle multiplicity without increasing the event number. Another package called SMASH [56] handles particle scattering as the fireball expands including their resonance decay. For this it solves a tower of Boltzmann equations,

$$p^\mu \partial_\mu f(u^\mu p_\mu) = C[f_i]. \quad (24)$$

Here  $C[f_i]$  is the collision term that encodes the scattering of particles of species  $i$ . All soft sector observables can be calculated from the energy and momenta of particles produced from the afterburner stage.

### III. MODEL PARAMETERS

The fluid description stops at particlization, and it turns out that the dissipative correction to the local equilibrium distribution for particles in Eq.(23) is non-trivial.

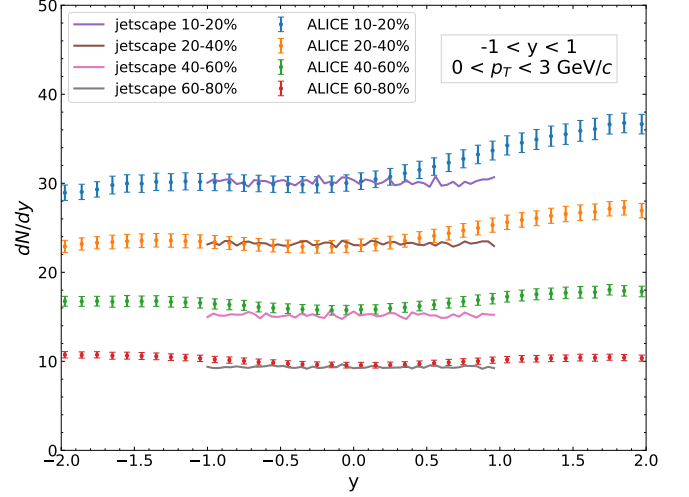


FIG. 2. Rapidity spectra of charged particles ( $\pi^\pm, K^\pm, p$ ) has been plotted for mentioned centralities. The experimental values taken from Ref. [57] are available for wider rapidity range, but simulated results for 2+1D system are only valid at midrapidity. Simulated data is scaled by a factor of 1.15.

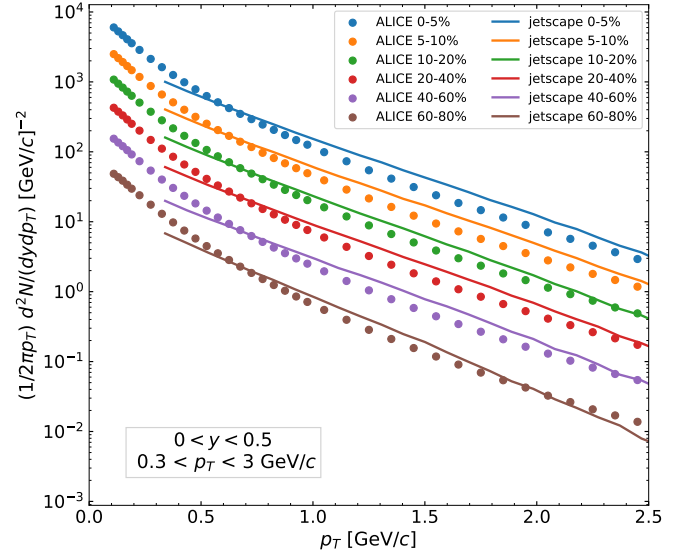


FIG. 3. Transverse momentum spectra of charged pions ( $\pi^+ + \pi^-$ ) has been plotted for mentioned centralities for  $0 < y < 0.5$  and  $0.3 < p_T < 3$  GeV/c. Experimental data is taken from Ref. [58]. Simulated data is scaled by a factor of 0.012.

This correction is a major source of uncertainty. A recent Bayesian study [36] for nucleus-nucleus collisions compared the 3 choices of this correction, which are: 14-moments or Grad's method [60], first-order Chapman-Enskog expansion in the relaxation time approximation [61, 62] and Pratt-Torrieri-Bernhard's modified equilibrium distribution [63, 64]. It is concluded that the light particle observables favor the Grad's and Pratt-Torrieri-Bernhard's correction terms relatively more. For the present study, we chose the set of constrained param-

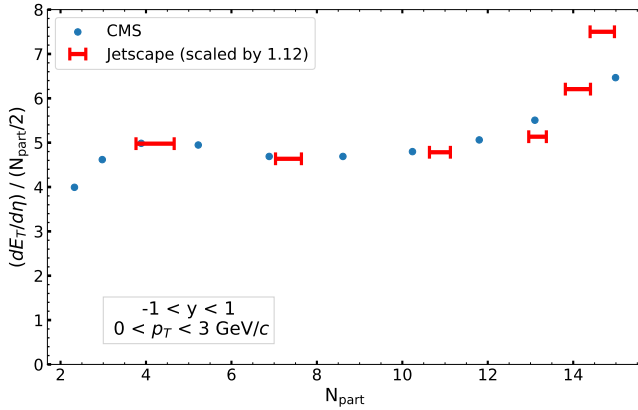


FIG. 4. Rapidity density per participating nucleon pair as a function of number of participants ( $N_{\text{part}}$ ). Experimental data is taken from Ref. [59].

ters centered around the Grad's method correction term as given in table II in Ref. [36]. Hence, we are assuming that the constrained parameter set for Pb-Pb can also be approximately utilized for the p-Pb system. The only value chosen that differs from this constrained parameters set is the Freestreaming time,  $\tau_{\text{fs}} = 1 \text{ fm}/c$ , which we expect to be shorter for a small system like p-Pb. The centrality values are set through percentage centrality bins in T<sub>RENT</sub>O. The input parameters for each of the models explained in Sec.II, have to be set for p-Pb collisions at 5.02 TeV. The kinematic cuts used for simulation are  $0 < p_T < 3 \text{ GeV}/c$  and  $-1 < y < 1$  for all observables, except for  $p_T$ -spectra as its experimental data uses the range  $0 < y < 0.5$ . The nucleon-nucleon collision cross section has been set to  $\sigma_{NN} = 67 \text{ mb}$  [65]. The normalization parameter for initial energy density is varied to match the generated charged particle rapidity spectra with experimental data as shown in Fig.2. The charged particles considered for analysis are pions, kaons, and protons as they are the most abundantly produced hadrons. As the simulated system is boost invariant 2+1 dimensional, we match it with experimental data near mid-rapidity.

Fig. 3 shows the generated  $p_T$ -spectra for charged pions compared with experimental data. As the yield of charged particles produced from the model does not match the experimental data, scaling had to be used in simulated data as stated in each plot.

Fig. 4 shows the charged particle rapidity spectra as a function of the number of participants. And one finds a good match between model and experimental data. The initial energy density is scaled such that the simulated rapidity spectra match with experimental data. The number of events set to produce observables for centrality from 0-5% to 85-95%, ranges from 1000 to 4000. The constraint for selecting these many events was the size of the data file produced and the computational time required for the simulation to run. For each event, hadrons are sampled 320 times from the freezeout surface to boost

(hadrons/event) which is a feature provided with the framework.

#### IV. RESULTS AND DISCUSSION

For finding the system size below which hydrodynamization breaks down, the basic idea is to vary the shear relaxation time ( $\tau_\pi$ ) for extreme values and to see its effect on the fluctuations in elliptic flow. An abrupt increase in deviation of elliptic flow towards peripheral collisions would signify the onset. The shear relaxation time is given by the Eq. 21. In a previous study [33], the shear relaxation time was varied through its normalization ( $b_\pi$ ) while keeping the shear viscosity to entropy density ratio a constant. Following the same process, we varied  $b_\pi$  between 2 to 8 whose value was otherwise set to be 4.65 in the Grad's parameter set.

Fig. 5 shows the elliptic flow curve for peripheral centrality bins plotted as a function of transverse momentum. We see the fluctuation in flow increasing towards the extreme peripheral collisions, which suggests the breakdown of hydrodynamic behavior. An envelop function for both of these extreme  $b_\pi$  value flow curves has also been plotted to highlight the increase in fluctuation.

Fig. 6 shows the envelop function for  $p_T$  integrated elliptic flow as a function of  $dN/dy$ . An abrupt increase in fluctuation of elliptic flow can be seen below the centrality range 75-85%, which is marked as a blue patch to highlight a transition region from a fluid-like regime to a parton scattering regime.

From Eq. 21, we notice that the shear relaxation time can also be varied if we change the shear viscosity to entropy density ratio, which in this study has been parameterized to be temperature dependent. This temperature dependence stated in Eq. 20 is a mean of the 90% credibility interval of the posteriors from the Bayesian analysis carried out in Ref. [36].

Fig. 7 shows the variation of  $\eta/s$  with temperature for different settings. The parameterization of  $\eta/s$  by the Grad's method is also shown in Fig. 7. To vary  $\eta/s$  in the extreme range, the upper 90% credibility Bayesian limit and a straight line near  $\eta/s = 1/4\pi$  were used. This lower limit is selected to respect the lower bound on  $\eta/s$  of strongly interacting matter obtained from AdS/CFT correspondence [66], also known as the KSS limit.

Fig. 8 shows the elliptic flow values for different centrality classes of peripheral collisions for varying shear relaxation time using extreme values of  $\eta/s$  while keeping the normalization value fixed at  $b_\pi = 4.65$ . We observe that the fluctuation envelop widens significantly towards peripheral collisions. Fig. 9 shows the  $p_T$  integrated elliptic flow envelop as a function of  $dN_{ch}/dy$ . Although an abrupt increase in fluctuation flow envelop was not found, the fluctuations begin to increase as one moves towards the extreme peripheral collisions.

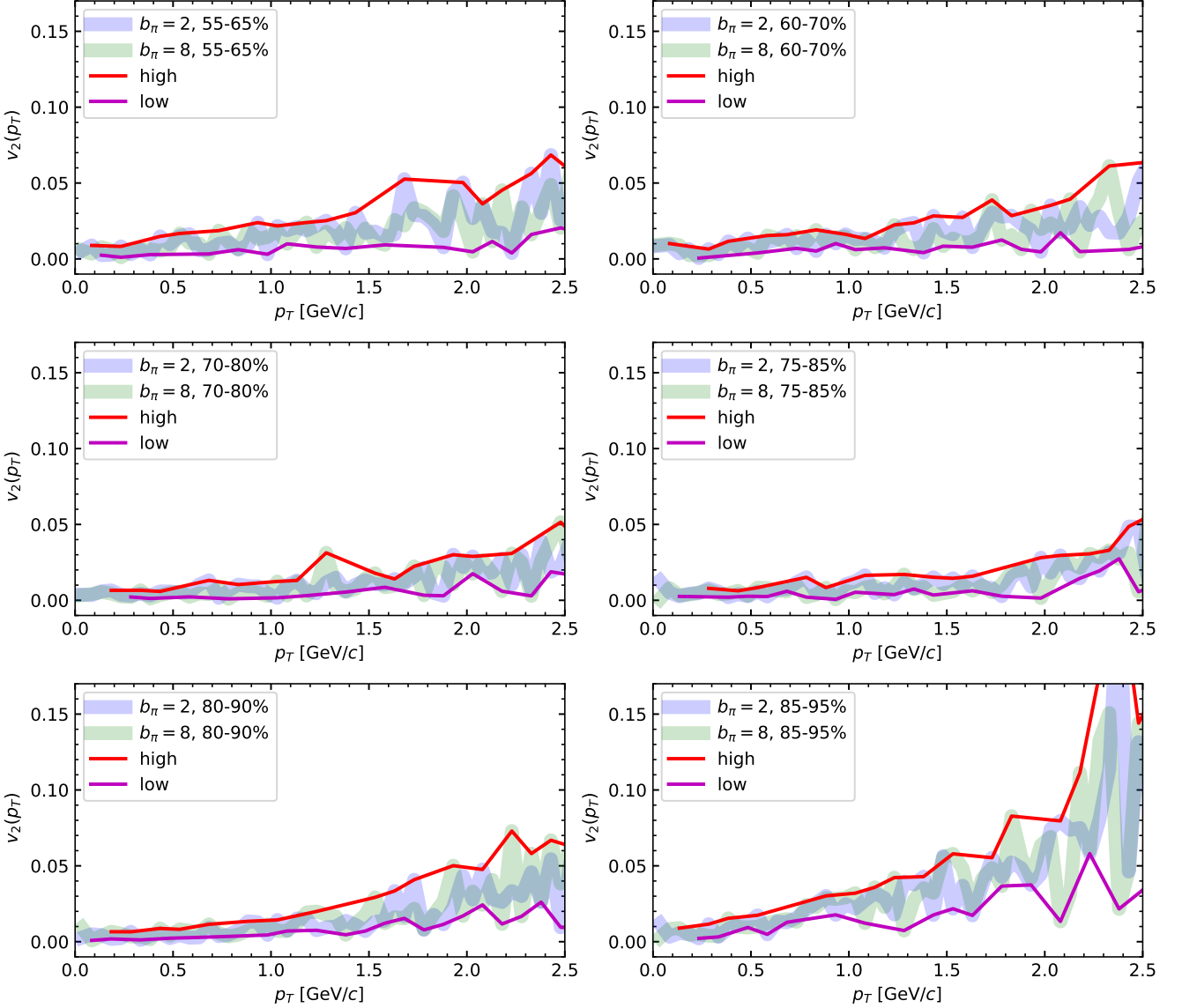


FIG. 5. The patched lines represent the elliptic flow values plotted as a function of transverse momentum for two extreme values of shear relaxation time normalization for peripheral collisions. The solid lines represent the higher and lower envelop of the fluctuation elliptic flow values. We notice that the fluctuation increases abruptly approximately below 75-85% centrality.

## V. CONCLUSION AND OUTLOOK

In an attempt to find the smallest system size of collision at which hydrodynamics would not be applicable in p-Pb collisions, the non-hydrodynamic mode regulated by the shear relaxation time of fluid dynamics was utilized. The shear relaxation time was varied in two ways, first using its constant normalization ( $b_\pi$ ) and then using the temperature-dependent  $\eta/s$  bounds. Based on the results obtained for elliptic flow as a function of transverse momentum and its fluctuation as a function of  $dN/dy$ , the following inferences can be drawn:

- A two times increase in flow fluctuation was observed as a function of  $dN/dy$ , indicating break-

down of hydrodynamic behavior below  $dN/dy \approx 7$  from Fig. 6 and significant increase below the value of  $dN/dy \approx 8$  for Fig. 9. Whether there exists a sharp onset or if there is a smooth transition region is still an open question.

- A large deviation of flow fluctuation was not seen below the inferred onset as was obtained in the previous study [33]. This could be due to multiple reasons: (1) An entirely different dynamic evolution was considered here, (2) The MUSIC viscous hydrodynamics used in the present work is relatively more stable than the previously employed ECHO-QGP as illustrated in Fig.(12) of Ref. [31].

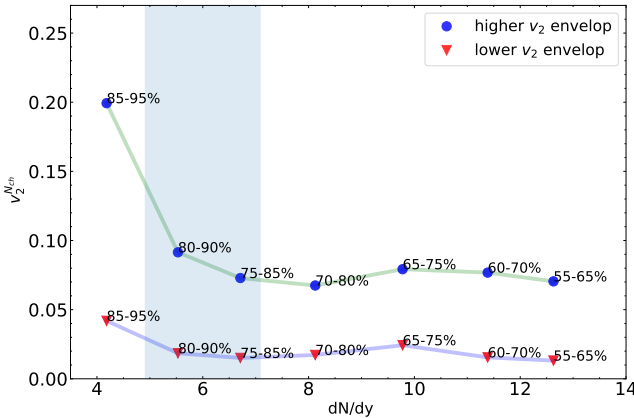


FIG. 6. Elliptic flow fluctuation envelopes for peripheral centrality is plotted as a function of rapidity density for varying shear relaxation time normalization. The data points are marks with centrality values. The blue patch represents the transition region for the onset of hydrodynamization.

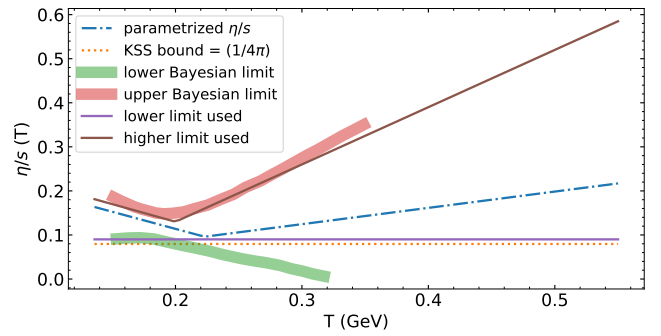


FIG. 7. Plot of different  $\eta/s$  parametrization. The green and red thick lines are the lower and upper 90% credibility intervals of the posteriors from the Bayesian study in Ref. [36]. The dot-dashed line is the plot for parametrization given in Eq. 20. Curves plotted “lower and higher limit used” are the curves used to vary  $\eta/s$  in the plots of Fig. 8 and 9.

The assumption that the soft sector can be investigated in isolation from hard sector in high energy collisions was more of a convenient approximation made in phenomenological studies, including this present study. Very few attempts have been made to explain both of these sectors simultaneously [67, 68]. The JETSCAPE framework has been designed to model hard and soft sectors simultaneously, including the interaction between them. One of the crucial QGP signatures that we have not discovered explicitly yet in small systems is jet quenching [4]. A right extension of this study would be to include a signature of onset from hard sector. It will be interesting to see how the inclusion of observables from the hard sector affects soft sector observables and vice versa.

#### ACKNOWLEDGMENTS

N.H. is grateful to Paul Romatschke, Chun Shen, Yasuki Tachibana and Scott Moreland for clearing various doubts from time to time. N. H. would also like to thank the Indian Institute of Technology Bombay for the financial support. S. D. acknowledges the SERB Power Fellowship, SPF/2022/000014 for the support in this work.

---

[1] P. Foka and M. A. Janik, An overview of experimental results from ultra-relativistic heavy-ion collisions at the CERN LHC: Bulk properties and dynamical evolution, *Rev. Phys.* **1**, 154 (2016).

[2] P. Foka and M. A. Janik, An overview of experimental results from ultra-relativistic heavy-ion collisions at the CERN LHC: Hard probes, *Rev. Phys.* **1**, 172 (2016).

[3] V. Khachatryan, A. M. Sirunyan, A. Tumasyan, W. Adam, T. Bergauer, M. Dragicevic, J. Erö, C. Fabjan, M. Friedl, R. Frühwirth, *et al.*, Observation of long-range, near-side angular correlations in proton-proton collisions at the LHC, *J. High Energy Phys.* **2010** (9), 1.

[4] J. L. Nagle and W. A. Zajc, Small System Collectivity in Relativistic Hadronic and Nuclear Collisions, *Annu. Rev. Nucl. Part. Sci.* , 211 (2018).

[5] K. Dusling, W. Li, and B. Schenke, Novel collective phenomena in high-energy proton-proton and proton-nucleus collisions, *International Journal of Modern Physics E* **25**, 1630002 (2016).

[6] Enhanced production of multi-strange hadrons in high-multiplicity proton-proton collisions (2017), [Online; accessed 30. Jul. 2024].

[7] (2024), [Online; accessed 30. Jul. 2024].

[8] J. Rafelski, Melting hadrons, boiling quarks, *Eur. Phys. J. A* **51**, 1 (2015).

[9] M. Strickland, Small system studies: A theory overview, *Nucl. Phys. A* **982**, 92 (2019).

[10] C. Alt *et al.* (NA49 Collaboration), Pion and kaon pro-

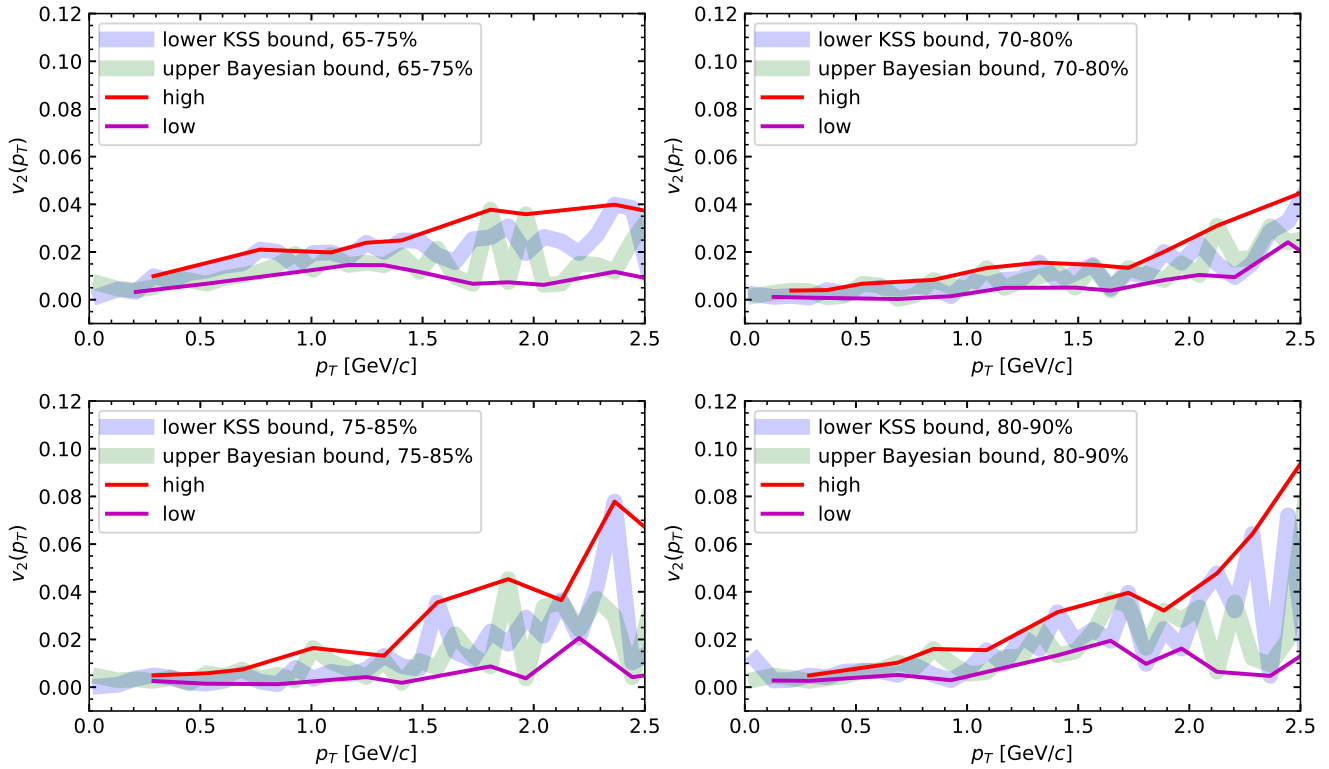


FIG. 8. The thick patched lines representing the elliptic flow values plotted as a function of transverse momentum for two extreme values of shear relaxation time by varying  $\eta/s$ . The solid lines represent the higher and lower envelop of the elliptic flow values.

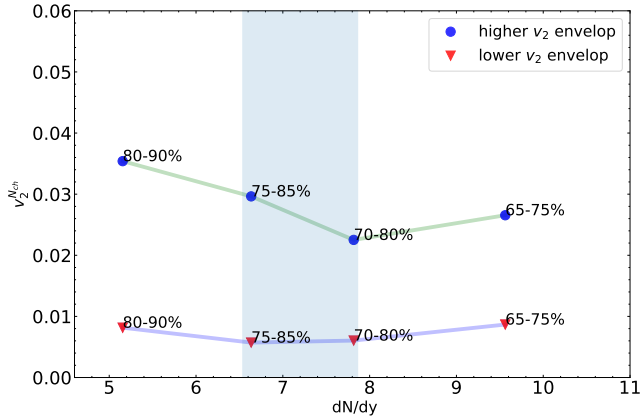


FIG. 9. Elliptic flow fluctuation envelopes for peripheral centrality are plotted as a function of rapidity density for the case when  $\eta/s$  is varied. The data points are marks with centrality values. The blue patch highlights the transition region for the onset of hydrodynamization.

duction in central Pb + Pb collisions at 20a and 30a gev: Evidence for the onset of deconfinement, Phys. Rev. C **77**, 024903 (2008).

[11] M. Gazdzicki, M. Gorenstein, and P. Seyboth, Onset of deconfinement in nucleus-nucleus collisions: Review for pedestrians and experts, Acta Physica Polonica B **42**,

10.5506/APhysPolB.42.307 (2011).

[12] C. Gale, S. Jeon, and B. Schenke, HYDRODYNAMIC MODELING OF HEAVY-ION COLLISIONS, Int. J. Mod. Phys. A **28**, 1340011 (2013).

[13] U. W. Heinz, Thermalization at RHIC, AIP Conf. Proc **739**, 163 (2004).

[14] P. Arnold, J. Lenaghan, G. D. Moore, and L. G. Yaffe, Apparent thermalization due to plasma instabilities in the quark-gluon plasma, Phys. Rev. Lett. **94**, 072302 (2005).

[15] M. P. Heller and M. Spaliński, Hydrodynamics beyond the gradient expansion: Resurgence and resummation, Phys. Rev. Lett. **115**, 072501 (2015).

[16] P. Romatschke, Do nuclear collisions create a locally equilibrated quark-gluon plasma?, Eur. Phys. J. C **77**, 1 (2017).

[17] Y. Akamatsu, Approach to thermalization and hydrodynamics, Nucl. Phys. A **1005**, 122000 (2021).

[18] R. Campanini and G. Ferri, Experimental equation of state in pp and  $pp^-$  collisions and phase transition to quark gluon plasma, Phys. Lett. B **703**, 237 (2011).

[19] A. Kurkela, U. A. Wiedemann, and B. Wu, Flow in AA and pA as an interplay of fluid-like and non-fluid like excitations, Eur. Phys. J. C **79**, 1 (2019).

[20] J. Casalderrey-Solana, M. P. Heller, D. Mateos, and W. van der Schee, Longitudinal coherence in a holographic model of asymmetric collisions, Phys. Rev. Lett. **112**, 221602 (2014).

[21] W. A. Hiscock and L. Lindblom, Generic instabilities

in first-order dissipative relativistic fluid theories, *Phys. Rev. D* **31**, 725 (1985).

[22] P. Kovtun, First-order relativistic hydrodynamics is stable, *J. High Energy Phys.* **2019** (10), 1.

[23] A. Pandya and F. Pretorius, Numerical exploration of first-order relativistic hydrodynamics, *Phys. Rev. D* **104**, 023015 (2021).

[24] I. Müller, Zum Paradoxon der Wärmeleitungstheorie, *Z. Phys.* **198**, 329 (1967).

[25] W. Israel, Nonstationary irreversible thermodynamics: A causal relativistic theory, *Ann. Phys.* **100**, 310 (1976).

[26] W. Israel and J. M. Stewart, Transient relativistic thermodynamics and kinetic theory, *Ann. Phys.* **118**, 341 (1979).

[27] G. S. Denicol, T. Koide, and D. H. Rischke, Dissipative relativistic fluid dynamics: a new way to derive the equations of motion from kinetic theory, *arXiv* 10.1103/PhysRevLett.105.162501 (2010), 1004.5013.

[28] W. Florkowski and R. Ryblewski, Highly anisotropic and strongly dissipative hydrodynamics for early stages of relativistic heavy-ion collisions, *Phys. Rev. C* **83**, 034907 (2011).

[29] R. Baier, P. Romatschke, D. T. Son, A. O. Starinets, and M. A. Stephanov, Relativistic viscous hydrodynamics, conformal invariance, and holography, *J. High Energy Phys.* **2008** (04), 100.

[30] A. Aduszkiewicz, Study of Hadron-Nucleus and Nucleus-Nucleus Collisions at the CERN SPS: Early Post-LS2 Measurements and Future Plans, CERN Document Server (2018).

[31] W. Florkowski, M. P. Heller, and M. Spaliński, New theories of relativistic hydrodynamics in the LHC era, *Rep. Prog. Phys.* **81**, 046001. (2018), 29225204.

[32] M. Spaliński, Small systems and regulator dependence in relativistic hydrodynamics, *Phys. Rev. D* **94**, 085002 (2016).

[33] N. Hatwar and M. Mishra, Using the nonhydrodynamic mode to study the onset of hydrodynamic behavior in ultraperipheral symmetric nuclear collisions, *Phys. Rev. C* **106**, 054902 (2022).

[34] J. H. Putschke *et al.*, The JETSCAPE framework, *arXiv* 10.48550/arXiv.1903.07706 (2019), 1903.07706.

[35] S. Cao *et al.* (JETSCAPE Collaboration), Determining the jet transport coefficient  $\hat{q}$  from inclusive hadron suppression measurements using bayesian parameter estimation, *Phys. Rev. C* **104**, 024905 (2021).

[36] D. Everett *et al.* (JETSCAPE Collaboration), Multisystem bayesian constraints on the transport coefficients of qcd matter, *Phys. Rev. C* **103**, 054904 (2021).

[37] A. Kumar *et al.* (JETSCAPE Collaboration), Inclusive jet and hadron suppression in a multistage approach, *Phys. Rev. C* **107**, 034911 (2023).

[38] W. Fan, G. Vujanovic, S. A. Bass, A. Majumder, *et al.* (JETSCAPE Collaboration), Multiscale evolution of charmed particles in a nuclear medium, *Phys. Rev. C* **107**, 054901 (2023).

[39] I. Soudi *et al.*, A soft-hard framework with exact four momentum conservation for small systems, *arXiv* 10.48550/arXiv.2407.17443 (2024), 2407.17443.

[40] <https://github.com/JETSCAPE/JETSCAPE/releases/tag/v3.6.4>.

[41] J. Liu, C. Shen, and U. Heinz, Pre-equilibrium evolution effects on heavy-ion collision observables, *Phys. Rev. C* **91**, 064906 (2015).

[42] J. S. Moreland, J. E. Bernhard, and S. A. Bass, Alternative ansatz to wounded nucleon and binary collision scaling in high-energy nuclear collisions, *Phys. Rev. C* **92**, 011901 (2015).

[43] M. Rybczyński and W. Broniowski, Wounded-nucleon model with realistic nucleon-nucleon collision profile and observables in relativistic heavy-ion collisions, *Phys. Rev. C* **84**, 064913 (2011).

[44] D. D'Enterria, G. Kh. Eyyubova, V. L. Korotkikh, I. P. Lokhtin, S. V. Petrushanko, L. I. Sarycheva, and A. M. Snigirev, Estimates of hadron azimuthal anisotropy from multiparton interactions in proton-proton collisions at  $\sqrt{s} = 14$  TeV, *Eur. Phys. J. C* **66**, 173 (2010).

[45] J. S. Moreland, Initial conditions of bulk matter in ultrarelativistic nuclear collisions, *arXiv* 10.48550/arXiv.1904.08290 (2019), 1904.08290.

[46] P. Bożek and W. Broniowski, Collective dynamics in high-energy proton-nucleus collisions, *Phys. Rev. C* **88**, 014903 (2013).

[47] B. Schenke, S. Jeon, and C. Gale, (3+1)d hydrodynamic simulation of relativistic heavy-ion collisions, *Phys. Rev. C* **82**, 014903 (2010).

[48] R. Baier, P. Romatschke, D. T. Son, A. O. Starinets, and M. A. Stephanov, Relativistic viscous hydrodynamics, conformal invariance, and holography, *J. High Energy Phys.* **2008** (04), 100.

[49] B. Schenke, C. Shen, and P. Tribedy, Running the gamut of high energy nuclear collisions, *Physical Review C* **102**, 044905 (2020).

[50] A. Bazavov, T. Bhattacharya, C. DeTar, H.-T. Ding, S. Gottlieb, R. Gupta, P. Hegde, U. M. Heller, F. Karsch, E. Laermann, L. Levkova, S. Mukherjee, P. Petreczky, C. Schmidt, C. Schroeder, R. A. Soltz, W. Soeldner, R. Sugar, M. Wagner, and P. Vranas (HotQCD Collaboration), Equation of state in (2 + 1)-flavor qcd, *Phys. Rev. D* **90**, 094503 (2014).

[51] G. S. Denicol, Kinetic foundations of relativistic dissipative fluid dynamics, *J. Phys. G: Nucl. Part. Phys.* **41**, 124004 (2014).

[52] J. E. Bernhard, J. S. Moreland, and S. A. Bass, Bayesian estimation of the specific shear and bulk viscosity of quark-gluon plasma, *Nat. Phys.* **15**, 1113 (2019).

[53] H.-T. Ding, New developments in lattice QCD on equilibrium physics and phase diagram, *Nucl. Phys. A* **1005**, 121940 (2021).

[54] F. Cooper and G. Frye, Single-particle distribution in the hydrodynamic and statistical thermodynamic models of multiparticle production, *Phys. Rev. D* **10**, 186 (1974).

[55] M. Mc Nelis, D. Everett, and U. Heinz, Particilization in fluid dynamical simulations of heavy-ion collisions: The iS3D module, *Comput. Phys. Commun.* **258**, 107604 (2021).

[56] J. Weil, V. Steinberg, J. Staudenmaier, L. G. Pang, D. Oliinychenko, J. Mohs, M. Kretz, T. Kehrenberg, A. Goldschmidt, B. Bäuchle, J. Auvinen, M. Attems, and H. Petersen, Particle production and equilibrium properties within a new hadron transport approach for heavy-ion collisions, *Phys. Rev. C* **94**, 054905 (2016).

[57] S. Acharya *et al.*, System-size dependence of the charged-particle pseudorapidity density at  $s_{NN}=5.02\text{TeV}$  for pp, pPb, and PbPb collisions, *Phys. Lett. B* **845**, 137730 (2023).

[58] B. Abelev *et al.*, Multiplicity dependence of pion, kaon,

proton and lambda production in p–Pb collisions at  $s_{NN}=5.02$  TeV, Phys. Lett. B **728**, 25 (2014).

[59] A. M. Sirunyan *et al.* (CMS Collaboration and CMS Collaboration), Centrality and pseudorapidity dependence of the transverse energy density in  $p$ Pb collisions at  $\sqrt{s_{NN}} = 5.02$  tev, Phys. Rev. C **100**, 024902 (2019).

[60] H. Grad, On the kinetic theory of rarefied gases, Commun. Pure Appl. Math. **2**, 331 (1949).

[61] S. Chapman, T. Cowling, and D. Park, The mathematical theory of non-uniform gases (1939), [Online; accessed 29. Jul. 2024].

[62] A. Jaiswal, R. Ryblewski, and M. Strickland, Transport coefficients for bulk viscous evolution in the relaxation-time approximation, Phys. Rev. C **90**, 044908 (2014).

[63] S. Pratt and G. Torrieri, Coupling relativistic viscous hydrodynamics to boltzmann descriptions, Phys. Rev. C **82**, 044901 (2010).

[64] J. E. Bernhard, Bayesian parameter estimation for relativistic heavy-ion collisions, arXiv 10.48550/arXiv.1804.06469 (2018), 1804.06469.

[65] C. Loizides, J. Kamin, and D. d'Enterria, Improved monte carlo glauber predictions at present and future nuclear colliders, Phys. Rev. C **97**, 054910 (2018).

[66] P. K. Kovtun, D. T. Son, and A. O. Starinets, Viscosity in strongly interacting quantum field theories from black hole physics, Phys. Rev. Lett. **94**, 111601 (2005).

[67] I. Lokhtin, L. Malinina, S. Petrushanko, A. Snigirev, I. Arsene, and K. Tywoniuk, Heavy ion event generator hydjet++ (hydrodynamics plus jets), Computer Physics Communications **180**, 779–799 (2009).

[68] K. Werner, B. Guiot, I. Karpenko, and T. Pierog, Analyzing radial flow features in  $p$ -pb and  $p$ - $p$  collisions at several tev by studying identified-particle production with the event generator epos3, Phys. Rev. C **89**, 064903 (2014).